Using airborne LiDAR to quantify changes in forest structure following an ice storm disturbance and subsequent salvage logging

Scandinavian Journal of Forest Research

ISSN: 0282-7581 (Print) 1651-1891 (Online) Journal homepage: www.tandfonline.com/journals/sfor20

Using airborne LiDAR to quantify changes in forest structure following an ice storm disturbance and subsequent salvage logging

Milan Kobal, Dejan Firm, Elena Belcore, Niccolò Marchi, Emanuele Lingua, Marco Piras & Thomas A. Nagel

To cite this article: Milan Kobal, Dejan Firm, Elena Belcore, Niccolò Marchi, Emanuele Lingua, Marco Piras & Thomas A. Nagel (29 Sep 2025): Using airborne LiDAR to quantify changes in forest structure following an ice storm disturbance and subsequent salvage logging, Scandinavian Journal of Forest Research, DOI: 10.1080/02827581.2025.2563602

To link to this article: https://doi.org/10.1080/02827581.2025.2563602

SCANDINAVIAN JOURNAL OF FOREST RESEARCH
https://doi.org/10.1080/02827581.2025.2563602

Taylor & Francis
Taylor & Francis Group

Using airborne LiDAR to quantify changes in forest structure following an ice storm disturbance and subsequent salvage logging

Milan Kobal[a], Dejan Firm[b], Elena Belcore[c], Niccolò Marchi[d], Emanuele Lingua[d], Marco Piras[c] and Thomas A. Nagel[a]

[a]Department for Forestry and Renewable Forest Resources, Biotechnical Faculty, University of Ljubljana, Ljubljana, Slovenia; [b]Bioeconomy Science Institute, Scion Group, Rotorua, New Zealand; [c]Department of Environment, Land and Infrastructure Engineering (DIATI), Politecnico di Torino, Torino, Italy; [d]Department Land, Environment, Agriculture and Forest (TESAF), University of Padova, Legnaro, Italy

ABSTRACT

Ice storms are common disturbance agents in temperate forests, often causing complex damage by partially destroying tree crowns. These irregular damage patterns pose challenges in production forests. Post-disturbance management decisions, such as salvage logging, are typically based on hastily collected field data, which is costly, time-consuming, and often fails to capture damage heterogeneity. Remote sensing offers a practical alternative. In 2014, a severe ice storm damaged mixed forests across the northern Dinaric Mountains. We used multitemporal high-density Airborne Laser Scanning data to validate a procedure for quantifying ice storm damage in stands dominated by Norway spruce, silver fir and European beech, using field data as a reference. LiDAR-derived leaf area density profiles and voxel-based biomass loss estimates effectively reflected field-observed patterns. Methods based on individual-tree segmentation underestimated post-disturbance tree density reductions, but basal area and volume loss estimates aligned closely with field measurements, even at low point densities. These methods offer a scalable approach to damage assessment and improve understanding of the spatial variability of ice storm impacts. They also hold considerable promise for land managers with access to regional bitemporal LiDAR datasets.

KEYWORDS

canopy dynamics; forest disturbance; remote sensing; airborne laser scanning; leaf area density; voxel-based analysis; point cloud density

Introduction

Many natural disturbances in forests often cause moderate or intermediate severity damage across a range of spatial scales (Frelich and Lorimer 1991; Woods 2004; Stueve et al. 2011; Nagel et al. 2017). Intermediate severity disturbances leave a lasting legacy on forest structure and dynamics, influencing carbon storage and primary production (Stuart-Haentjens et al. 2015; Woods and Kern 2022), structural complexity (Meigs and Keeton 2018; Fahey et al. 2020), community composition (Woods 2000; Nagel et al. 2014), and habitat conditions for biodiversity (Kozák et al. 2021). A common characteristic of intermediate severity disturbances includes "messy" and heterogenous damage patterns over space, ranging from crown damage of individual trees to scattered gaps and larger patches of canopy removal that can retain some live trees (Greenberg and McNab 1998; Woods 2004; Nagel and Diaci 2006; Hanson and Lorimer 2007).

Although a number of different disturbance agents can cause intermediate severity damage to forests (Atkins et al. 2020), ice storms, in particular, often create remarkably complex damage patterns – mainly because, in addition to snapping and uprooting entire trees, they cause partial damage to the crowns of otherwise living stems, ranging from the removal of small branches to nearly entire crowns (Rebertus et al. 1997; Irland 2000; Duguay et al. 2001; Isaacs et al. 2014; Nagel et al. 2016). Moreover, the meteorological conditions that give rise to ice storms often occur over large spatial scales, such that damage to forests can occur over 100s-1000s of km^2 (Changnon 2003).

Ice storms are relatively common disturbance agents in many temperate forest regions (Rebertus et al. 1997; Proulx and Greene 2001; Changnon 2003; Zhou et al. 2011; Nagel et al. 2016). Consequently, their large size and complex damage patterns also create several unique challenges where forests are regularly managed for timber production. For example, management decisions immediately following natural disturbances, such as sanitary and salvage logging operations,

CONTACT Milan Kobal milan.kobal@bf.uni-lj.si Department for Forestry and Renewable Forest Resources, Biotechnical Faculty, University of Ljubljana, Večna pot 83, Ljubljana SI-1000, Slovenia

Supplemental data for this article can be accessed online at https://doi.org/10.1080/02827581.2025.2563602.

are largely based on data that is hastily collected in the field, yet it is costly, time-consuming, and difficult to accurately quantify heterogeneous and complex damage patterns across large forested regions. Moreover, post-ice storm management may include salvage logging of live trees with partial crown damage that may otherwise survive (Bragg et al. 2003; Nyland et al. 2016; Roženbergar et al. 2020), as well as sanitary logging of damaged trees of target species to prevent pest outbreaks (de Groot et al. 2018). As such, it is important for managers to quantify the outcome and effectiveness of post-disturbance management operations, both as a basis for further management planning and to assess potential forest recovery patterns.

Remote sensing methods provide a clear solution to many of the challenges associated with quantifying post-ice storm changes in forest structure. Remotely sensed data can improve the decision-making process by reducing the response time of managers, covering large landscapes with less cost, and improving objectivity and accuracy of the quantification of damage patterns and post-disturbance forest structure. In particular, airborne laser scanning (ALS) using Light Detection and Ranging (LiDAR) technology has the advantage of capturing large areas with the sufficiently high resolution (Coops et al. 2009; Wulder et al. 2012) needed to detect the fine-scale damage patterns characteristic of ice storms. However, very few studies have examined the utility of ALS for quantifying ice-storm damage in forests. Previous work using either ALS or terrestrial laser scanning (TLS) in forests affected by ice storms has examined stand scale changes in forest structural complexity (Atkins et al. 2020; Fahey et al. 2020), characteristics of canopy gaps (Liu et al. 2020), and landscape scale severity patterns (Anderson et al. 2011). However, we are not aware of any studies quantifying fine-scale changes in forest structure before, immediately after ice storm damage, and following post-ice storm salvage logging operations.

In 2014, a large and intense ice storm caused intermediate and heterogenous damage patterns to temperate forests in Slovenia (Nagel et al. 2016; Nagel et al. 2017), a region with a long history of continuous cover forest management aimed toward sustainable timber production (Bončina 2011). Silvicultural prescriptions, including the annual allowable harvest, follow strict management plans in Slovenia, but natural disturbances often damage a substantial portion of the timber that would otherwise be harvested under regular silvicultural plans (Štraus and Bončina 2025). As such, accurate assessment of damage patterns following disturbance is required to readjust long-term planning and for salvage logging operations. The main objective of this study was to assess the impact of a severe ice storm event on stand structural changes in managed mixed-mountain forests and compare structural changes derived from field-based measurements and airborne laser scanning data. We examine several measures of structural change and assess how point cloud density influences the comparison to field-based measurements. Specifically, the study aims to:

1. Assess post-storm reduction in tree density, basal area, and growing stock for the main tree species.
2. Assess post-storm changes in stand-level structure.
3. Examine if pre- and post-storm leaf area density can be used to detect canopy structure changes.
4. Evaluate the reliability of voxel-based estimates in measuring aboveground biomass loss post-ice storm and salvage logging.
5. Evaluate the accuracy of LiDAR-derived change detection in tree density, basal area, and growing stock across different point cloud densities, using field measurements as a reference.

Materials and methods

Description of the study area

The study was carried out in the Snežnik forest management unit (FMU Snežnik) in the Dinaric Mountain region of southern Slovenia (Figure 1). The landscape is characterized by typical high-karst features, with Leptosols, Cambisols, and Luvisols as the predominant soil types. The region has a humid temperate climate with an average annual rainfall of 1642 mm and an average annual temperature of 6.6 °C (ARSO 2025). During the extended winter period (November to March), the study area receives 690 mm (42%) of precipitation (Meteorological station Babno Polje). Forest communities are dominated by three main tree species, namely, European beech (*Fagus sylvatica* L.), silver fir (*Abies alba* Mill.) and Norway spruce (*Picea abies* (L.) H. Karst.). Sycamore maple (*Acer pseudoplatanus* L.), wych elm (*Ulmus glabra* Huds.), common ash (*Fraxinus excelsior* L.), and lime (*Tilia cordata* Mill.) are present sporadically. The mean growing stock of the studied forests is 442 m^3 ha^{-1} and the mean annual increment is 8.3 m^3 ha^{-1} yr^{-1} (SFS - FMP 2015). In the last 40 years, the structure and composition of the forest have changed due to the chronic decline of silver fir and forest management practices that favored uneven-aged forest stands, resulting in high structural diversity. The study site (45.672° N, 14.460° E) is located at an altitude of 750–870 m and covers approximately 70 ha.

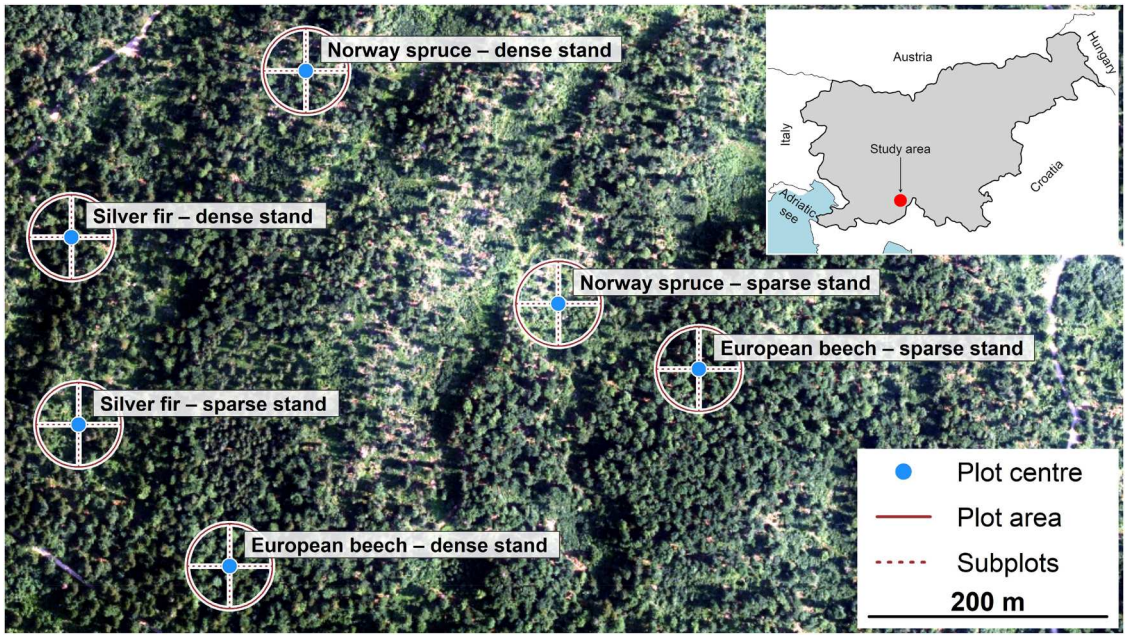

Figure 1. Location and arrangement of the research plots within the study area. The circles represent individual forest plots (blue dot = centre of the plot; red circle = area of the plot; red dashed crosses = subplots). The inset map shows the location of the study area in Slovenia. Imagery was taken after the ice storm and salvage logging.

The 2014 ice storm and its impact on the FMU Snežnik

In 2014, between 30 January and 5 February, a large-scale and intense ice storm caused damage to more than 600,000 hectares of forest in Slovenia (SFS - FMP 2015; Figure 2) and Croatia. In the most intense areas, the precipitation exceeded 350 mm (URSZR 2018) and ice thickness on flat surfaces was between 50 and 90 mm in some regions (Mezgec 2015). Forest damage was most severe at elevations between 300 and 1,200 m. Salvage logging began immediately after the ice storm in February 2014 and continued in 2015 due to a bark beetle outbreak.

Establishment of research plots and pre/post-ice storm tree measurements

In 2011, six research plots were established at the Snežnik trial site as part of the Life + ManFor C.BD project (LIFE09 ENV/IT/000078 2010-2015). Three plots had a dense (closed) canopy, while the other three plots had a sparse (open) canopy. The plots were distributed across stands with different tree species composition: two plots were located in Norway spruce-dominated stands (spruce-dominated stand), two in silver fir-dominated stands (fir-dominated stand) and two in European beech-dominated stands (beech-dominated stand).

The plots were circular with an area of 4000 m^2 (radius of 35.7 m). In each plot, tree locations (x, y) were measured with a Leica TS12 total station. The diameter at breast height (at 1.3 m above ground level; DBH) of all live trees (DBH $\geq$ 10 cm) was measured and the tree species was recorded (n = 681). Tree height (H) was measured on a sub-sample of trees in a 10 m wide strip, oriented north to south through the center of the plot. We used this data to develop species-specific height curves.

All plots were re-measured in 2013, four months before the ice storm. After the 2014 storm, once the salvage logging was completed, the plots were remeasured again and the locations of the stumps of salvaged trees were recorded. Mainly trees that were uprooted or snapped during the ice storm were salvage logged, while trees that only had damaged crowns were retained.

Estimation of tree attributes from field measurements

Based on the height data from the sub-sample of trees in each plot, we created site-specific height curves for each species in order to estimate the tree height values not measured in the field. The basal area (BA) of each tree was calculated using standard equations, while the volume (V) and aboveground biomass (AGB) were calculated from DBH, H and tree species data using library "rBDAT" (Kublin 2003) in R software (R Core Team 2024) using function *getVolume* (coarse wood volume over bark from forest floor up to diameter over bark of 7 cm) and *getBiomass* (total aboveground biomass), respectively.

Figure 2. Typical ice storm damage in one of the research plots, characterized by broken and uprooted trees, mainly silver fir (*Abies alba* Mill.), and extensive accumulation of both fine and coarse woody debris on the forest floor.

Airborne laser scanning data acquisition

The ALS data acquisition was performed in November 2013, April 2014, and October 2014 (Figure S1; Figure S2; Figure S3). All three data acquisitions were conducted while the deciduous species, European beech, was without foliage, i.e. under leaf-off conditions. The broader study site was surveyed using a Eurocopter EC 120B helicopter equipped with a Riegl LMS5600 laser scanner. The scanner has a relative horizontal accuracy of 10 cm and a relative vertical accuracy of 3 cm. It operates at a wavelength of 1550 nm, has a maximum effective measurement range of up to 1100 m, depending on atmospheric conditions and the reflectivity of the target, and can record multiple echoes per pulse. The original point cloud densities before downscaling were 130.9 points m^{-2} (November 2013), 319.4 points m^{-2} (April 2014), and 164.7 points m^{-2} (October 2014).

Point cloud subsampling and density variation

The processing and analyses that follow were performed on preprocessed point clouds, i.e. classified, and ground normalized in a second step. To compare field-based measurements with ALS data for assessing changes in stand structure after the ice storm and salvage logging, we applied the same analytical procedure using three different point cloud densities: high point density, medium point density and low point density.

Downscaling was performed using the *Subsample* function in CloudCompare software (CloudCompare 2025) with the spatial subsampling method. This algorithm thins the original point cloud by enforcing a minimum distance between retained points. It processes the cloud sequentially, retaining the first point and then evaluating each subsequent point; a point is kept only if no previously retained point lies within the specified distance. The output is a reduced point cloud of the desired density (CloudCompare 2025). The minimum point distance was set to 0.1 m for high point density (resulted in mean point density of 97.6 points m^{-2}), 0.8 m for medium density (resulted in mean point density of 5.1 points m^{-2}), and 1.2 m for low point density (resulted in mean point density of 2.4 points m^{-2}).

LiDAR-based analysis of forest structural changes

Our study employs several different metrics to compare LiDAR- and field-based measurements of forest change following the ice storm event and subsequent post-disturbance management. These metrics, which can be used for large-area forest structure characterizations, span from coarser-scale estimates of canopy structure, such as changes in leaf area density (e.g. Coops et al.

2009; Bouvier et al. 2015; Kamoske et al. 2019), to finer-scale attributes that capture individual-tree level changes in biomass, diameter, basal area, and volume. The latter are derived using voxel-based metrics and segmentation of individual-tree crowns. Each approach is described in more detail below.

Estimation of leaf area density

Leaf area density (LAD) was calculated from the highest-density point cloud using the approach described by Bouvier et al. (2015), based solely on first and single LiDAR returns. The LAD was calculated in 1 m height bins to produce a detailed vertical profile of canopy structure at three different time points. Since the LiDAR data were collected during the leaf-off season, the LAD values determined for European beech should be interpreted as a structural proxy reflecting the woody elements (branches and stems) and not the actual leaf area density. No correction was made to estimate leaf-on LAD, and this limitation is acknowledged in the discussion.

To ensure accuracy, only points within a scan angle of ±23° were used, as recommended by Liu et al. (2018). Larger angles beyond the nadir are associated with lateral penetration of the tree crowns and are not suitable for a metric intended to represent vertical structure. The calculation of LAD, implemented in the library "lidR" (Roussel and Auty 2017) in R software (R Core Team 2024), is based on the gap fraction profile, which estimates the number of laser pulses that reached a given layer $z + dz$ and the number of pulses that traversed the layer $[z, z + dz]$. The logarithm of the ratio between these two values is then divided by the extinction coefficient k to obtain an estimate of the LAD for each vertical segment (Bouvier et al. 2015).

Voxel-based assessment of aboveground biomass changes

To assess aboveground biomass changes (AGB), we computed voxel representations of the normalized ALS point clouds using the *voxel_metrics* function from the "lidR" package in R software (R Core Team 2024), with a voxel resolution of $1 \times 1 \times 1$ m. The voxel-based metrics were calculated separately for ALS datasets acquired in November 2013 (pre-ice storm) and October 2014 (post-salvage logging), based solely on highest-density point cloud. By comparing the voxel layers from both November 2013 and October 2014, we identified three voxel classes: a) voxels that were present in both years (vx_{common}), b) voxels that were only present in 2013 before the ice storm and absent in 2014 after salvage logging (vx_{lost}), and c) voxels that appeared in 2014 but were absent in 2013 (vx_{new}).

Tree segmentation and tree attribute estimation from ALS data

Individual-tree segmentation of the point cloud data was performed using the approach proposed by Dalponte and Coomes (2016), applied to the ALS datasets from November 2013 and October 2014. The segmentation was based on a canopy height model (CHM) for each ALS data acquisition separately, with a pixel size of 0.5 m with pit-free algorithm developed by Khosravipour et al. (2014). Individual-tree segmentation was performed with the "lidR" package (Roussel and Auty 2017) using the *dalponte2016* function in R software (R Core Team 2024).

For each segmented tree in the ALS data, H was derived directly from the normalised LiDAR point cloud. The crown radius was estimated from the convex hull of the segmented crown, which was also obtained from the ALS data. The DBH was then estimated using the allometric model of Jucker et al. (2017), which relates H and crown radius to the DBH. Based on the estimated DBH, the BA of each tree was calculated. Volume was estimated using the procedure described in section 2.3.1. The tree species identity for each ALS-segmented tree was assigned based on the dominant tree species observed in the respective plot from the field data. To investigate the effect of LiDAR point density on the evaluation of changes in basic stand structure characteristics (tree density, basal area and growing stock), we used three different point densities (see Section 2.4.1) and performed tree segmentation and attribute extraction separately for each.

Statistical modeling and data analysis

Linear mixed models (LMMs) were used to evaluate how well LiDAR-derived voxel loss explained variation in field calculated aboveground biomass change (ΔAGB) following the 2014 ice storm. The standardized lost voxel volume (vx_{lost}) was included as a fixed effect, and *plot* was modeled as a random intercept to account for variability among the six plots. Although each plot was divided into four subplots, there was no replication at the subplot level, and a simplified hierarchical model was applied:

$$\Delta AGB_{ij} = \beta_0 + \beta_1 vx_{lost} + b_j + \varepsilon_{ij}$$

where:

- ΔAGB_{ij} predicted aboveground biomass change in subplot i of plot j
- β_0 model intercept
- β_1 fixed effect of voxel volume loss vx_{lost}
- b_j random effect of plot

- ε_{ij} residual error

LMMs were also used to evaluate the performance of LiDAR-derived tree density, basal area and growing stock compared to field measurements. This was carried out using metrics derived from 3 different point cloud densities, to ascertain the importance of point cloud density. The inventory method (field-based and ALS-derived estimates using high, medium and low point density) was treated as a categorical fixed effect. Random effects accounted for the nested structure of the data:

$$Y_{ijk} = \beta_0 + \beta_1 \text{method}_i + b_k + b_{kj} + \varepsilon_{ijk}$$

where:

- Y_{ijk} predicted structural metric (tree density, basal area, growing stock) for inventory method$_i$, subplot j, plot k
- β_0 model intercept
- β_1 fixed effect of inventory method (low, medium, high)
- b_k, b_{kj} random effects for plot and subplot (nested)
- ε_{ijk} residual error

Models were implemented in R using the lme4 package (Bates et al. 2015), using the *lmer* function with restricted maximum likelihood estimation and Satterthwaite approximation for p-values. Pseudo-R-squared for Generalized Mixed-Effect models was calculated using the *r.squaredGLMM* function in the MuMIn package (Bartoń 2024). To examine differences between levels of point cloud density factor, estimated marginal means (EMMs) were calculated using the emmeans package (Lenth 2025) and *emmeans* function.

Results

Changes in tree-level structure after the ice storm and salvage logging

In total, the number of live trees declined from 2013 to 2014 (Table 1) due to the combined effects of the ice storm and salvage logging, with Norway spruce experiencing the greatest relative decline (50.3%), while silver fir and European beech showed smaller declines (26.6% and 20.9%, respectively).

In 2013, the mean diameter (DBH = 39.3 cm) and mean volume (V = 2.0 m^3) were highest for silver fir, while the lowest values were observed for European beech (DBH = 30.6 cm, V = 1.3 m^3). The greatest mean height (H = 26.0 m) was observed for Norway spruce. In 2014, the average values changed due to the mortality and removal of trees damaged by the ice storm. An increase in mean tree DBH and V was observed in all three tree species. The greatest increase in mean height (H = 28.5 m) occurred for Norway spruce, while for populations of silver fir and European beech only minor changes in mean tree height were detected, although both species showed an increase in mean tree volume. For trees removed due to ice storm damage, mean DBH and tree height were lower compared to surviving trees. For the trees that were salvage logged after the ice storm, Norway spruce trees had a mean DBH of 31.2 cm and a mean volume of 1.1 m^3, which were substantially lower than the values determined for the surviving trees in 2014. Even lower values were recorded for silver fir and European beech.

Table 1. Mean diameter at breast height (DBH), height (H) and volume (V) (mean ± 95% confidence interval) of all live trees censused in 2013 and 2014 and of trees that were removed due to ice storm (salvage logging). The n represents the number of trees recorded in each category; data were pooled across all six plots.

Year	Tree species	n	DBH (cm)	H (m)	V (m^3)
2013	Norway spruce	177	36.3 ± 1.8	26.0 ± 1.0	1.5 ± 0.2
	Silver fir	184	39.3 ± 2.5	24.2 ± 1.1	2.0 ± 0.2
	European beech	320	30.6 ± 1.5	24.8 ± 0.7	1.3 ± 0.2
2014	Norway spruce	89	41.4 ± 2.4	28.5 ± 1.2	1.9 ± 0.2
	Silver fir	135	40.2 ± 2.9	24.7 ± 1.3	2.1 ± 0.3
	European beech	253	32.1 ± 1.7	25.4 ± 0.7	1.4 ± 0.2
Salvage cut	Norway spruce	88	31.2 ± 2.3	23.4 ± 1.5	1.1 ± 0.2
	Silver fir	49	36.7 ± 5.1	22.9 ± 2.5	1.8 ± 0.5
	European beech	67	25.1 ± 2.6	22.5 ± 1.3	0.8 ± 0.3

Changes in stand-level structure after the ice storm and salvage logging

Across all stand types, tree density, basal area, and growing stock decreased from 2013 to 2014 due to mortality and salvage logging following ice storm damage (Table 2). The greatest decline was observed in the spruce-dominated stands, where tree density dropped from 371 trees ha^{-1} in 2013 to 208 trees ha^{-1} in 2014 (a decrease of 44%). The basal area and growing stock in the spruce-dominated stands also decreased by 35% and 33%, respectively. There were also reductions in stand parameters in silver fir- and beech-dominated stands, albeit to a lesser extent. The tree density of silver fir-dominated stands decreased by 24%, the basal area and growing stock by 19%. Beech-dominated stands showed the smallest overall decline: tree density and basal area declined by 14% and growing stock by 13%. The lowest number of trees removed during salvage cutting was recorded in the beech-dominated stands (39 trees ha^{-1}), followed by fir-dominated

Table 2. Mean tree density, basal area, and growing stock for Norway spruce-, silver fir- and European beech-dominated stands in 2013 and 2014 and for trees removed due to ice break (salvage logging). The values represent the mean ± 95% confidence interval for each category.

Year	Stand	Tree density (n ha^{-1})	Basal area (m^2 ha^{-1})	Growing stock (m^3 ha^{-1})
2013	Norway spruce-dominated	371 ± 147	35.7 ± 9.9	469.2 ± 130.1
	Silver fir-dominated	226 ± 59	30.3 ± 7.2	427.2 ± 112.3
	European beech-dominated	254 ± 61	27.8 ± 5.3	416.4 ± 82.2
2014	Norway spruce-dominated	208 ± 95	23.2 ± 8.6	314.0 ± 116.6
	Silver fir-dominated	171 ± 60	24.4 ± 9.3	347.4 ± 142.4
	European beech-dominated	218 ± 51	24.0 ± 2.9	361.1 ± 40.2
Salvage cut	Norway spruce-dominated	164 ± 73	12.5 ± 3.7	155.2 ± 43.7
	Silver fir-dominated	55 ± 18	5.9 ± 3.5	79.8 ± 49.8
	European beech-dominated	36 ± 22	3.8 ± 3.4	55.2 ± 52.0

stands (65 trees ha^{-1}) and spruce-dominated stands (164 trees ha^{-1}).

Leaf area density (LAD) profiles before and after the ice storm and salvage logging

The profile of LAD shows considerable variation among stands before the ice storm, following the ice storm, and after salvage logging (Figure 3). In some stands the LAD was distinctly concentrated in the upper part of the vertical profile, like in beech-dominated sparse stands, while silver fir showed a more even distribution both in dense and sparse stands. Fir-dominated stands were the least damaged by the ice storm and few trees were felled as part of the salvage cutting. Beech-dominated stands suffered considerable damage to tree crowns (Figure S4), but in most cases, the damaged trees were not removed. In the case of spruce-dominated stands, the direct impact of the ice storm was relatively small, but the subsequent salvage logging was intense, resulting in a significant decrease in the LAD profile.

Voxel-based estimation of aboveground biomass loss after the ice storm and salvage logging

The linear mixed-effects model showed a strong and statistically significant positive relationship between the standardized vx_{lost} and AGB loss (Table 3; Figure 4). Specifically, the fixed effect estimate for vx_{lost} was 2645.1 ($p = 0.0022$), indicating that for each unit increase in standardised voxel loss, aboveground biomass decreased by approximately 2645.1 kg or for each voxel loss 1.52 kg. The model intercept was estimated at 4954.5 ($p = 0.0030$).

The random effects show that considerable variability exists between the forest plots (plot). The marginal R^2 ($R2m = 0.470$) shows that the fixed effect alone explains about 47% of the variance in biomass change, while the conditional R^2 ($R2c = 0.635$) shows that the full model, including the random effects, explains about 64% of the total variance.

Changes in stand structure after the ice storm and salvage logging: comparison of field-based and LiDAR-based estimates

The analysis comparing the tree density reduction estimates between field measurements and the LiDAR-based method revealed significant differences (Table 4; Figure 5). The intercept value of -9.0 ($p = 0.0023$) represents the average reduction in tree density as determined by field-based measurements. When comparing LiDAR-derived estimates with field-based measurements, all point density methods systematically underestimated tree density reduction (Table 4), while the difference among LiDAR-derived estimates was not statistically significant ($p > 0.05$). The results also showed variability in the severity of damage among the different plots (plot_group, variance = 16.72), suggesting that the extent of tree density reduction varies across the study area. In addition, variability was also observed at the sub-plot level (plot_group: subplot, variance = 2.99), suggesting that damage was not spatially uniform even within individual plots.

The analysis of basal area reduction revealed no statistically significant differences between LiDAR-based methods and the field-based reference measurements (Table 4; Figure 5). The intercept value of -0.78 ($p = 0.002$) reflects the average reduction in basal area as recorded by field-based measurements. None of the LiDAR-based methods differed significantly from the field-based estimates, and moreover, no statistically significant differences ($p > 0.05$) were detected among LiDAR-derived estimates from different point cloud densities. The results also showed variability in the severity of basal area reduction among different plots (plot_group, variance = 0.10), and within plots at the sub-plot level (plot_group:subplot, variance = 0.10).

The analysis of growing stock reduction revealed statistically non-significant differences between LiDAR-

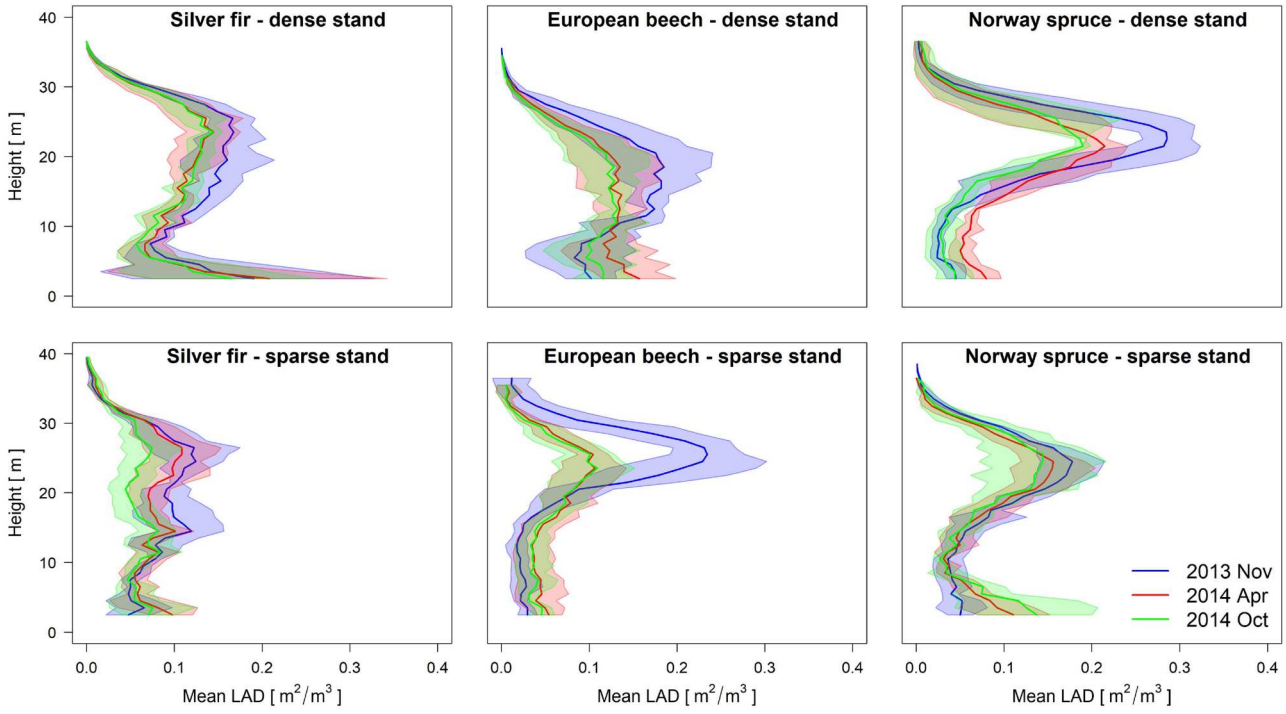

Figure 3. Vertical profiles of mean Leaf Area Density (LAD) across canopy height for three time points: blue lines represent the average LAD before the ice storm (November 2013), red lines show LAD after the storm (April 2014), and green lines represent LAD after salvage logging operations were completed (October 2014).

based methods and the field-based reference measurements (Table 4; Figure 5). The intercept value of -10.27 ($p = 0.007$) reflects the average volume reduction as recorded by field-based measurements. The results also showed variability in the severity of volume reduction among plots (plot_group, variance = 22.22), and within plots (plot_group:subplot, variance = 21.92). Additionally, the post-hoc pairwise comparisons showed no statistically significant differences in growing stock estimates between the three point cloud densities (all $p > 0.05$). This confirms that growing stock change can be reliably estimated even from lower-density point clouds.

Discussion

The airborne laser scanning performed reasonably well for capturing changes in forest structure following the ice-storm and post-storm salvage logging, but performance varied depending on the specific LiDAR-derived metric, highlighting both the utility and limitations of LiDAR-based approaches. Moreover, for some metrics in particular, such as changes to the basal area and growing stock, low resolution LiDAR data performed as well as high resolution data, which is an encouraging result given that low resolution data is more likely to be available over large forested areas and requires less computational resources for processing and data storage.

The post-storm reduction in tree density, basal area, and growing stock for the main tree species is consistent with other independent assessments of damage patterns following the 2014 ice storm event. Notably beech, and broadleaf species in general, were among the most susceptible to severe ice damage (Figure S4), while fir and spruce were least susceptible (Nagel et al. 2016). Nagel et al. (2016) also found that crown damage was common for beech, particularly for smaller sized trees and at low to intermediate levels of storm intensity. They also reported that larger trees were more susceptible to uprooting, which is consistent with field observations at our study site, where some of the larger spruce and fir trees uprooted or snapped during the ice storm (Figure 2). These damage patterns are reflected in the vertical profiles of leaf area density in April 2014, with the beech stands tending to show the highest level of canopy loss at canopy heights,

Table 3. Results of the linear mixed-effects model relating voxel loss (vx_{lost}) to aboveground biomass loss (ΔAGB).

Effect	Estimate	Std. Error	p value
Intercept	4954.5	796.98	0.0030
vx_{lost}	2645.1	685.49	0.0022

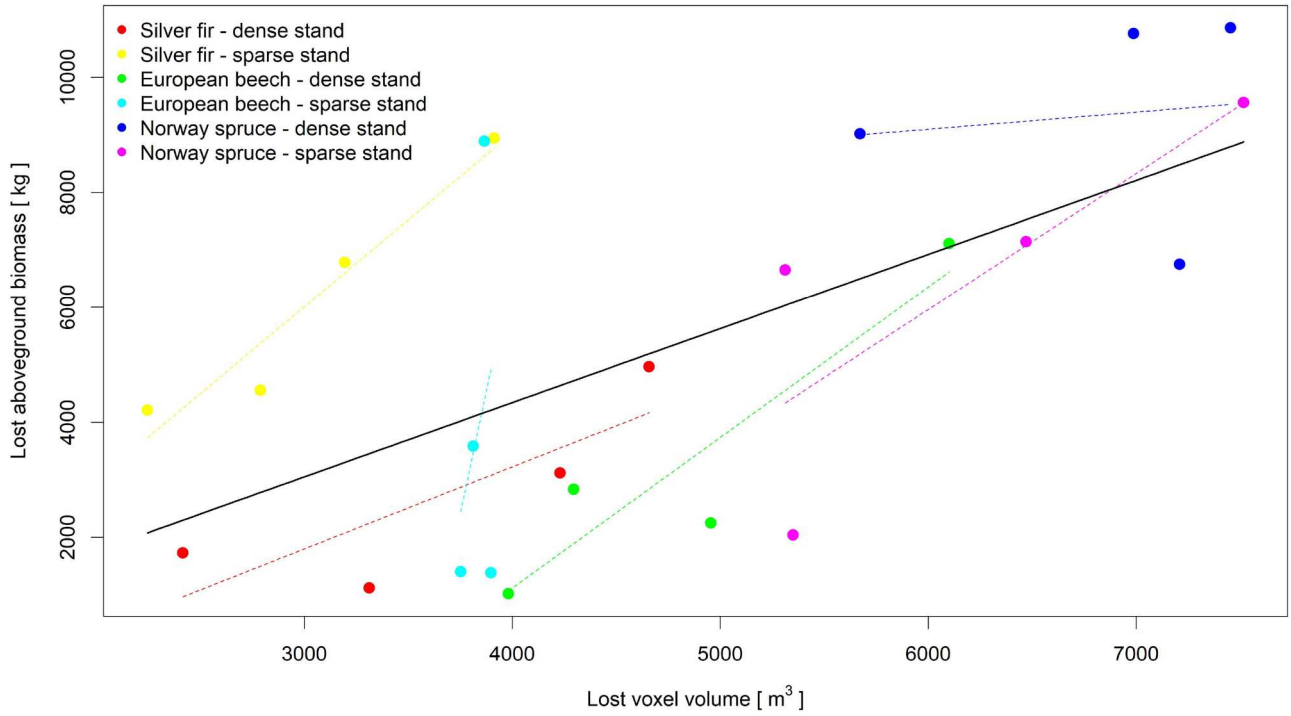

Figure 4. Relationship between the voxel-based volume loss and the loss in aboveground biomass (AGB) in the forest subplots. Colored dots represent individual observations in the subplots grouped by plot. Dashed regression lines show linear trends within each plot, while the solid black line shows the overall trend across all plots. The mixed-effects model includes voxel loss as a fixed effect and accounts for variability between plots through a random intercept for the plot.

with broken canopy material moving to lower heights near ground level post-ice storm. However, it is important to note that the LiDAR data were acquired during the leaf-off season, which means that the reported LAD values predominantly reflect woody structural elements (e.g. branches and stems) and cannot be directly compared in absolute terms to leaf-on data. While absolute differences between leaf-on and leaf-off plant area density profiles can be very large, relative changes (e.g. before and after a disturbance) are still valid and informative (Arnqvist et al. 2020).

Table 4. Linear mixed-effects model of tree density, basal area and growing stock reduction comparing field-based and LiDAR-based estimates with varying point densities. Non-significant p values are bold.

Stand structure parameter	Effect	Estimate	Std. Error	p value
Tree density	Intercept	-9.00	1.88	0.0023
	High point density	9.80	1.10	< 0.0001
	Medium point density	9.60	1.10	< 0.0001
	Low point density	9.00	1.10	< 0.0001
Basal area	Intercept	-0.78	0.15	0.0020
	High point density	0.11	0.08	**0.1711**
	Medium point density	0.05	0.08	**0.0561**
	Low point density	0.05	0.08	**0.5504**
Growing stock	Intercept	-10.26	2.34	0.0039
	High point density	-0.98	1.32	**0.4558**
	Medium point density	-2.15	1.32	**0.1065**
	Low point density	-1.84	1.32	**0.1663**

Post-storm salvage logging was also consistent with management recommendations following natural disturbances in Slovenia and Central Europe (Stadelmann et al. 2013; Leverkus et al. 2021). Uprooted or snapped trees, regardless of species, are typically removed for economic reasons, while damaged but living stems of spruce are routinely removed to limit subsequent bark beetle outbreaks. The post-salvage logging structure was relatively well captured by the LAD profile approach. Spruce shows lower values in the canopy, reflecting the large amount of spruce removed from the stands, while beech-dominated stands show a minor difference between the post-ice storm and post-salvage logging LAD profiles. Fir-dominated dense stands had minimal post-disturbance intervention, yet the changes in LAD profiles in sparse silver fir stands were more similar to those observed in spruce-dominated stands and can be attributed to the higher number of large silver fir trees that were either uprooted, snapped at the base, or lost their tops during the ice storm.

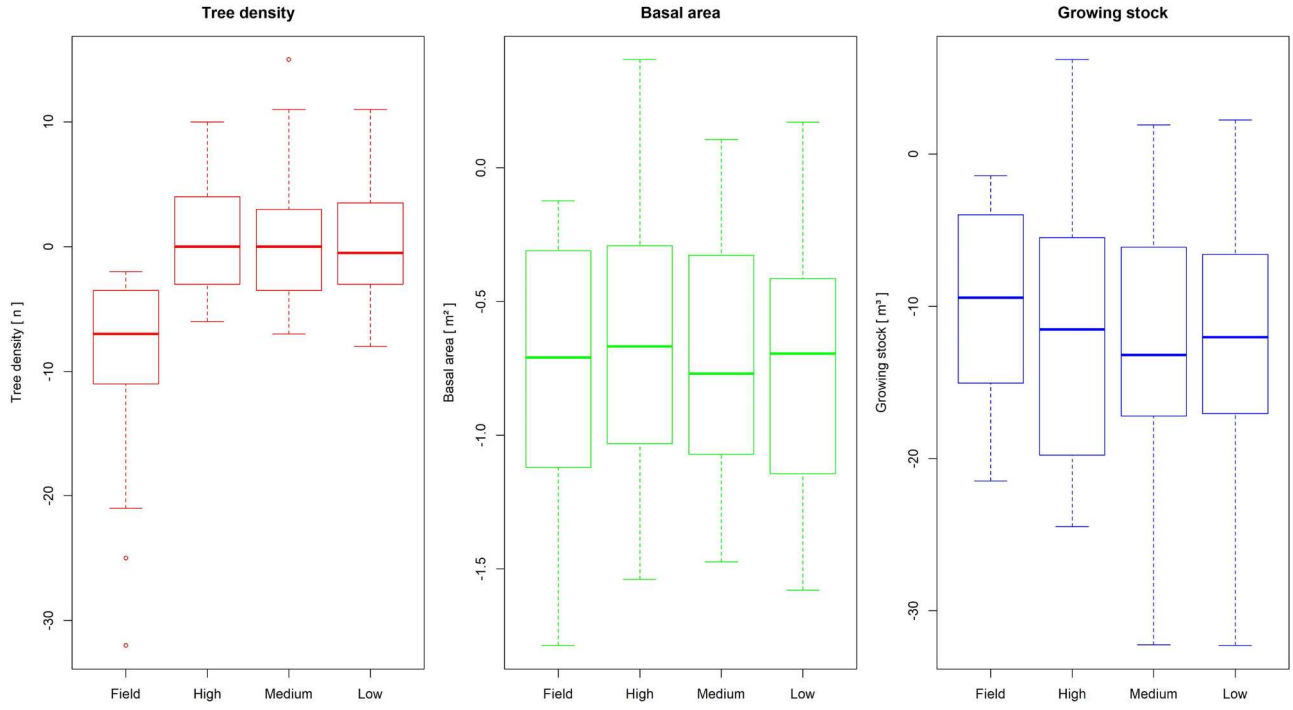

Figure 5. Comparison of tree density, basal area and growing stock reduction estimates across inventory methods after the ice storm and salvage logging.

The voxel-based approach also performed well in capturing loss of biomass, confirming that voxel-based metrics are robust predictors of aboveground biomass change (Skowronski et al. 2014). However, the chosen voxel size (i.e. 1 m^3) used for the documented relationship between voxel- and AGB-loss may be too coarse to capture some of the damage caused by the ice storm, which is, in combination with the cloud point density, likely one of the reasons for the high variability in the effect estimates. Voxel size is a key parameter in the voxelization of point clouds, as it strongly influences shape recognition, surface recognition and computational efficiency (Vosselman et al. 2004). A voxel size that is too fine can lead to data redundancy and high processing overhead (Ross et al. 2022), while a size that is too coarse can cause information loss and combine different structures within a single voxel (Lecigne et al. 2017). Therefore, the choice of voxel size depends on the research objective, object complexity and LiDAR platform (Béland et al. 2014; Wang and Fang 2020). For our study, a sensitivity analysis was performed with three voxel sizes (i.e. 0.5 m, 1 m and 2 m), which showed consistent results across the three resolutions. For clarity and comparability with other studies, a voxel size of 1 m^3 was used for all analyses. Overall, these results are promising and support the applicability of the tested method, yet finer resolutions may yield improved outcomes in some cases.

The results comparing the LiDAR-derived changes in tree density, basal area, and growing stock based on individual-tree segmentation with field-based measurements were mixed. LiDAR underestimated the reduction in tree density at all point cloud densities. The estimated tree density can be influenced by many sources of error, particularly the segmentation process. Top down algorithms, such as watershed based (Li et al. 2012), are known to perform better within conifer stands due to their conical architecture. When compared to the method proposed by Li et al. (2012), the watershed-based algorithms suffer from a strictly 2D approach related to the use of a rasterized canopy model to segment the point-cloud below and lack the ability to identify co-dominant and understory trees. Identification is even more challenging in damaged stands, where trees no longer have clearly defined crowns, whereby damaged trees may lose the seed point (i.e. treetop) and this may lead to a different segmentation output.

In contrast to density estimates, the LiDAR-derived estimates of basal area and volume loss closely matched the field-based measurements across all point densities. Tree density estimates often have the lowest precision compared to other standard forest inventory parameters (Pearse et al. 2019). Attributes like basal area and volume are less sensitive to the problems associated with individual-tree identification, likely

because the small trees in the understory that were difficult to identify do not have a large influence on these estimates. Given that the estimates of basal area and volume loss also hold for lower resolutions, they hold promise for land managers who may have access to national or regional scale bitemporal LiDAR datasets, which are becoming more readily available but often have lower point densities.

While there are few studies that allow direct comparison to our results, airborne laser scanning has been shown to effectively detect snow-induced forest disturbances through indicators such as reduced canopy height, changes in vertical structure, and formation of canopy gaps (Vastaranta et al. 2011; Vastaranta et al. 2012; Räty et al. 2024). These changes can be quantified using bitemporal or unitemporal ALS datasets and expressed via metrics derived from canopy height models (CHMs) or percentile-based height distributions (Vastaranta et al. 2012; Nyström et al. 2013; Marchi et al. 2018). Given that ice storms induce similar mechanical damage to tree crowns compared to heavy, wet snow (Bragg et al. 2003; Beach et al. 2010), these ALS-derived indicators may be transferable for detecting ice-related damage to forests.

Although LiDAR shows promise for detecting ice storm damage and subsequent salvage logging, our study has several limitations that deserve attention. Most notably, our case study is based on a relatively small sampling area (i.e. six 0.4 ha plots within a 70 ha study area) with a heterogeneous forest structure, such that caution should be exercised when generalizing the results beyond our study area. There are also some methodological challenges that need further consideration. The point density used to estimate leaf area density (LAD) may not have been sufficient to completely resolve the vertical structure of the canopy, especially in complex, multi-layered, dense forest stands and in leaf-off conditions (Arnqvist et al. 2020; Halubok et al. 2021). Similarly, voxel-based analyses of canopy change rely on a level of structural detail that is difficult to achieve with medium-density point clouds, which could compromise the accuracy of derived estimates of aboveground biomass loss (Skowronski et al. 2014; Lecigne et al. 2017). As the focus of this study was not on testing different individual segmentation algorithms, we did not assess the accuracy of segmentation of individual trees and therefore cannot judge how well ALS-derived tree-level structural metrics reflect actual conditions, especially in damaged or suppressed crowns. The commonly used Dalponte method (Dalponte and Coomes 2016), which is based on local maxima in the canopy height model, can cause problems in forests affected by crown breakage or partial canopy loss (Spadavecchia et al. 2022), as is typical after ice storms. In addition, DBH estimates based on crown diameter become less reliable when crowns are deformed by ice storm damage, which further complicates the accuracy of predicting volume and total aboveground biomass (Réjou-Méchain et al. 2015). Finally, some of the derived tree-level attributes (e.g. V, AGB), obtained through either individual-tree segmentation or voxel-based estimation are subject to a degree of uncertainty, primarily because species identity was assigned rather than empirically verified. This remains a key limitation of ALS-based inventories – and LiDAR-based methods more broadly – as species differentiation continues to pose a significant challenge, particularly in compositionally diverse forests.

In summary, the results obtained are promising and support the use of ALS over large forested areas for post-disturbance assessment, especially for evaluating volume and basal area changes. In particular, the finding that lower-density ALS data can produce results comparable to those of high-density data is especially promising. This suggests that the effects of disturbance can be reliably quantified using existing operational LiDAR programmes, reducing costs and facilitating large-scale monitoring and decision-making in forest management. Challenges still remain, such as underestimation of stem density, likely due to the missed detection of broken or damaged codominant and understory trees. In this context, final consideration should be given to the down sampling technique adopted to evaluate the performance of point cloud-based algorithms at lower densities. It is important to note that in low density real-case scenarios, point density may not be homogeneously distributed but instead concentrated on the canopy surface. This depends on the type of LiDAR sensor used (e.g. number of returns, acquisition system, flight altitude and speed) and on the stand structure, which affects the ability of the LiDAR signal to penetrate the canopy. In conclusion, our results require further verification in different forest ecosystems. We therefore hope this work will inspire further research on the use of LiDAR methods to quantify ice storm damage to forest ecosystems.

Acknowledgements

This research was funded by Interreg Alpine Space project "Managing prOtective foreSt fAcIng cIImate Change compound events – MOSAIC" (ASP0100014) (https://www.alpine-space.eu/project/mosaic/) and the Slovenian Research and Innovation Agency (https://www.aris-rs.si/sl/) Program and Research Core Funding No. P4-0059 (MK, TAN) and by a

research Grant from the Man-For C. BD. (LIFE 09 ENV/IT/000078). LiDAR data and field data was acquired by the Slovenia Forestry Institute projects. The APC was funded by Pahernik foundation. D.F. was supported by Scion's Strategic Science Investment Funding from the New Zealand Ministry of Business, Innovation and Employment.

Disclosure statement

No potential conflict of interest was reported by the author(s).

References

Anderson JE et al. 2011. Use of waveform lidar and hyperspectral sensors to assess selected spatial and structural patterns associated with recent and repeat disturbance and the abundance of sugar maple (*Acer saccharum* Marsh.) in a temperate mixed hardwood and conifer forest. J Appl Remote Sens. 5(1):053504. https://doi.org/10.1117/1.3554639

Arnqvist J, Freier J, Dellwik E. 2020. Robust processing of airborne laser scans to plant area density profiles. Biogeosciences. 17:5939–5952. https://doi.org/10.5194/bg-17-5939-2020

ARSO. 2025. ARHIV - opazovani in merjeni meteorološki podatki po Sloveniji. https://meteo.arso.gov.si/met/sl/archive/

Atkins JW et al. 2020. Application of multidimensional structural characterization to detect and describe moderate forest disturbance. Ecosphere. 11(6):e03156. https://doi.org/10.1002/ecs2.3156

Bartoń K. 2024. MuMIn: Multi-Model Inference (Version 1.48.4) [R package]. https://CRAN.R-project.org/package=MuMIn

Bates D, Mächler M, Bolker B, Walker S. 2015. Fitting linear mixed-effects models using lme4. J Stat Softw. 67(1):1–48. https://doi.org/10.18637/jss.v067.i01

Beach RH, Sills EO, Liu T-M, Pattanayak S. 2010. The influence of forest management on vulnerability of forests to severe weather. In: Pye J.M., Rauscher H.M., Sands Y., Lee D.C., Beatty J.S., editor. Advances in threat assessment and their application to forest and rangeland management. Gen. tech. Rep. PNW-GTR-802. U.S. Department of Agriculture, Forest Service, Pacific Northwest and Southern Research Stations; p 185–206.

Béland M, Baldocchi DD, Widlowski J-L, Fournier RA, Verstraete M. 2014. On seeing the wood from the leaves and the role of voxel size in determining leaf area distribution of forests with terrestrial LiDAR. Agric For Meteorol. 184:82–97. https://doi.org/10.1016/j.agrformet.2013.09.005

Bončina A. 2011. History, current status and future prospects of uneven-aged forest management in the Dinaric region: an overview. For Int J For Res. 84(5):467–478. https://doi.org/10.1093/forestry/cpr023

Bouvier M, Durrieu S, Fournier RA, Renaud JP. 2015. Generalizing predictive models of forest inventory attributes using an area-based approach with airborne LiDAR data. Remote Sens Environ. 156:322–334. https://doi.org/10.1016/j.rse.2014.10.004

Bragg DC, Shelton MG, Zeide B. 2003. Impacts and management implications of ice storms on forests in the southern United States. For Ecol Manag. 186:99–123. https://doi.org/10.1016/S0378-1127(03)00230-5

Changnon SA. 2003. Characteristics of ice storms in the United States. J Appl Meteorol. 42:630–639. https://doi.org/10.1175/1520-0450(2003)042<0630:COISIT>2.0.CO;2

CloudCompare. 2025. CloudCompare (Version 2.14.alpha) [Computer software]. http://www.cloudcompare.org

Coops NC et al. 2009. Assessing differences in tree and stand structure following beetle infestation using lidar data. Can J Remote Sens. 35:497–508. https://doi.org/10.5589/m10-005

Dalponte M, Coomes DA. 2016. Tree-centric mapping of forest carbon density from airborne laser scanning and hyperspectral data. Methods Ecol. Evol. 7:1236–1245. https://doi.org/10.1111/2041-210X.12575

de Groot M, Ogris N, Kobler A. 2018. The effects of a large-scale ice storm event on the drivers of bark beetle outbreaks and associated management practices. For Ecol.Manage. 408:195–201. https://doi.org/10.1016/j.foreco.2017.10.035

Duguay SM, Arii K, Hooper M, Lechowicz MJ. 2001. Ice storm damage and early recovery in an old-growth forest. Environ Monit Assess. 67:97–108. https://doi.org/10.1023/A:1006464511158

Fahey RT et al. 2020. Effects of an experimental ice storm on forest canopy structure. Can J For Res. 50(2):136–145. https://doi.org/10.1139/cjfr-2019-0276

Frelich LE, Lorimer CG. 1991. Natural disturbance regimes in hemlock hardwood forests of the upper great-lakes region. Ecol Monogr. 61:145–164. https://doi.org/10.2307/1943005

Greenberg CH, McNab WH. 1998. Forest disturbance in hurricane-related downbursts in the Appalachian mountains of North Carolina. For Ecol Manage. 104:179–191. https://doi.org/10.1016/S0378-1127(97)00246-6

Halubok M, Kochanski AK, Stoll R, Bailey BN. 2021. Errors in the estimation of leaf area density from aerial LiDAR data: influence of statistical sampling and heterogeneity. IEEE Trans Geosci Remote Sens. 60:1–14. https://doi.org/10.1109/TGRS.2021.3123585

Hanson JJ, Lorimer CG. 2007. Forest structure and light regimes following moderate wind storms: implications for multi-cohort management. Ecol Appl. 17:1325–1340. https://doi.org/10.1890/06-1067.1

Irland LC. 2000. Ice storms and forest impacts. Sci Total Environ. 262:231–242. https://doi.org/10.1016/S0048-9697(00)00525-8

Isaacs RE, Stueve KM, Lafon CW, Taylor AH. 2014. Ice storms generate spatially heterogeneous damage patterns at the watershed scale in forested landscapes. Ecosphere. 5:141. https://doi.org/10.1890/ES14-00234.1

Jucker T et al. 2017. Allometric equations for integrating remote sensing imagery into forest monitoring programmes. Glob Chang Biol. 23:177–190. https://doi.org/10.1111/gcb.13388

Kamoske AG, Dahlin KM, Stark SC, Serbin SP. 2019. Leaf area density from airborne LiDAR: comparing sensors and resolutions in a temperate broadleaf forest ecosystem. For Ecol Manage. 433:364–375. https://doi.org/10.1016/j.foreco.2018.11.017

Khosravipour A, Skidmore AK, Isenburg M, Wang T, Hussin YA. 2014. Generating pit-free canopy height models from airborne lidar. Photogramm Eng Remote Sens. 80:863–872. https://doi.org/10.14358/PERS.80.9.863

Kozák D et al. 2021. Historical disturbances determine current taxonomic, functional and phylogenetic diversity of saproxylic beetle communities in temperate primary forests. Ecosystems. 24:37–55. https://doi.org/10.1007/s10021-020-00502-x

Kublin E. 2003. Einheitliche Beschreibung der Schaftform – Methoden und Programme – BDATPro. Forstwiss. Cent.bl. 122:183–200. https://doi.org/10.1046/j.1439-0337.2003.00183.x

Lecigne B, Delagrange S, Messier C. 2017. Exploring trees in three dimensions: VoxR, a novel voxel-based R package dedicated to analysing the complex arrangement of tree crowns. Ann Bot. 121:589–601. https://doi.org/10.1093/aob/mcx095

Lenth RV. 2025. emmeans: Estimated marginal means, aka least-squares means (Version 1.11.0) [R package]. https://CRAN.R-project.org/package=emmeans

Leverkus AB et al. 2021. Tamm review: does salvage logging mitigate subsequent forest disturbances? For Ecol Manage. 481:118721. https://doi.org/10.1016/j.foreco.2020.118721

Li W, Guo Q, Jakubowski MK, Kelly M. 2012. A new method for segmenting individual trees from the lidar point cloud. Photogramm Eng Remote Sens. 78:75–84. https://doi.org/10.14358/PERS.78.1.75

Liu F, Yang Z, Zhang G. 2020. Canopy gap characteristics and spatial patterns in a subtropical forest of south China after ice storm damage. J Mt Sci. 17:1942–1958. https://doi.org/10.1007/s11629-020-6020-8

Liu J et al. 2018. Large off-nadir scan angle of airborne LiDAR can severely affect the estimates of forest structure metrics. ISPRS J Photogramm Remote Sens. 136:13–25. https://doi.org/10.1016/j.isprsjprs.2017.12.004

Marchi N, Pirotti F, Lingua E. 2018. Airborne and terrestrial laser scanning data for the assessment of standing and lying deadwood: current situation and new perspectives. Remote Sens. 10:1356. https://doi.org/10.3390/rs10091356

Meigs GW, Keeton WS. 2018. Intermediate-severity wind disturbance in mature temperate forests: legacy structure, carbon storage, and stand dynamics. Ecol Appl. 28:798–815. https://doi.org/10.1002/eap.1691

Mezgec I. 2015. O nastanku žleda, in: Mednarodna konferenca Obnova gozdov po žledu, Postojna, 19–20. marec 2015 (in Slovene).

Nagel TA, Diaci J. 2006. Intermediate wind disturbance in an old-growth beech-fir forest in southeastern Slovenia. Can J For Res. 36:629–638. https://doi.org/10.1139/x05-263

Nagel TA, Firm D, Roženbergar D, Kobal M. 2016. Patterns and drivers of ice storm damage in temperate forests of central Europe. Eur J For Res. 1–12. https://doi.org/10.1007/s10342-016-0950-2

Nagel TA et al. 2017. The natural disturbance regime in forests of the Dinaric mountains: A synthesis of evidence. For Ecol Manage. 388:29–42. https://doi.org/10.1016/j.foreco.2016.07.047

Nagel TA, Svoboda M, Kobal M. 2014. Disturbance, life history traits, and dynamics in an old-growth forest landscape of Southeastern Europe. Ecol Appl. 24:663–679. https://doi.org/10.1890/13-0632.1

Nyland RD, Dalton JL, Allen DC, Bevilacqua E. 2016. Response of ice-damaged northern hardwood stands in northern New York. For Chron. 92:77–89. https://doi.org/10.5558/tfc2016-020

Nyström M, Holmgren J, Olsson H. 2013. Change detection of mountain birch using multi-temporal ALS point clouds. Remote Sens Lett. 4(2):190–199. https://doi.org/10.1080/2150704X.2012.714087

Pearse GD, Watt MS, Dash JP, Stone C, Caccamo G. 2019. Comparison of models describing forest inventory attributes using standard and voxel-based lidar predictors across a range of pulse densities. Intern J Appl Earth Observ Geoinform. 78:341–351.

Proulx OJ, Greene DF. 2001. The relationship between ice thickness and northern hardwood tree damage during ice storms. Can J For Res. 31:1758–1767. https://doi.org/10.1139/cjfr-31-10-1758

R Core Team. 2024. R: A language and environment for statistical computing. R Foundation for Statistical Computing. https://www.R-project.org/

Räty J, Kukkonen M, Melin M, Maltamo M, Packalen P. 2024. Detection of snow disturbances in boreal forests using uni-temporal airborne lidar data and aerial images. For Int J For Res. https://doi.org/10.1093/forestry/cpae057

Rebertus AJ, Shifley SR, Richards RH, Roovers LM. 1997. Ice storm damage to an old-growth oak-hickory forest in Missouri. Am Midl Nat. 137:48–61. https://doi.org/10.2307/2426754.

Réjou-Méchain M, et al. 2015. Using repeated small-footprint LiDAR acquisitions to infer spatial and temporal variations of a high-biomass Neotropical forest. Remote Sens Environ. 169:93–101. https://doi.org/10.1016/j.rse.2015.08.001

Ross CW et al. 2022. LiDAR voxel-size optimization for canopy gap estimation. Remote Sens. 14:1054. https://doi.org/10.3390/rs14051054

Roussel J-R, Auty D. 2017. lidR: Airborne LiDAR Data Manipulation and Visualization for Forestry Applications. [Software package].

Roženbergar D, Pavlin J, Nagel TA. 2020. Short-term survival and crown rebuilding of European broadleaf tree species following a severe ice storm. Can J For Res. 50:1131–1137. https://doi.org/10.1139/cjfr-2020-0063

SFS - FMP. 2015. Forest management plan for Forest Management Unit Snežnik 2015–2024, 342 p. (in Slovene).

Skowronski NS, Clark KL, Gallagher M, Birdsey RA, Hom JL. 2014. Airborne laser scanner-assisted estimation of aboveground biomass change in a temperate oak-pine forest. Remote Sens Environ. 151:166–174. https://doi.org/10.1016/j.rse.2013.12.015

Spadavecchia C, Belcore E, Piras M, Kobal M. 2022. An automatic individual tree 3D change detection method for allometric parameters estimation in mixed uneven-aged forest stands from ALS data. Remote Sens. 14:4666. https://doi.org/10.3390/rs14184666

Stadelmann G, Bugmann H, Meier F, Wermelinger B, Bigler C. 2013. Effects of salvage logging and sanitation felling on bark beetle (*Ips typographus* L.) infestations. For Ecol Manag. 305:273–281.

Štraus H, Bončina A. 2025. The vulnerability of four main tree species in European forests to seven natural disturbance agents: lessons from Slovenia. Eur J For Res. https://doi.org/10.1007/s10342-024-01754-1

Stuart-Haentjens EJ, Curtis PS, Fahey RT, Vogel CS, Gough CM. 2015. Net primary production of a temperate deciduous forest exhibits a threshold response to increasing

disturbance severity. Ecology. 96:2478–2487. https://doi.org/10.1890/14-1810.1

Stueve KM et al. 2011. Ecological importance of intermediate windstorms rivals large, infrequent disturbances in the northern great lakes. Ecosphere. 2:1–21. https://doi.org/10.1890/ES10-00062.1

URSZR. 2018. Ocena ogroženosti Republike Slovenije zaradi žleda. Ministrstvo za obrambo, Uprava Republike Slovenije za zaščito in reševanje, 54 str. https://www.gov.si/assets/organi-v-sestavi/URSZR/Datoteke/Ocene-ogrozenosti/ocena_ogrozenosti_zled.pdf (in Slovene).

Vastaranta M, Korpela I, Uotila A, Hovi A, Holopainen M. 2011. Area-based snow damage classification of forest canopies using bi-temporal lidar data. ISPRS Arch. XXXVIII-5/W12:169–173. https://doi.org/10.5194/isprsarchives-XXXVIII-5-W12-169-2011

Vastaranta M, Korpela I, Uotila A, Hovi A, Holopainen M. 2012. Mapping of snow-damaged trees based on bitemporal airborne LiDAR data. Eur J For Res. 131:1217–1228. https://doi.org/10.1007/s10342-011-0593-2

Vosselman G, Gorte BGH, Sithole G, Rabbani T. 2004. Recognising structure in laser scanner point clouds. ISPRS Archives. XXXVI-8/W2:33–38. http://www.isprs.org/proceedings/XXXVI/8-W2/VOSSELMAN.pdf

Wang Y, Fang H. 2020. Estimation of LAI with the LiDAR technology: A review. Remote Sens. 12:3457. https://doi.org/10.3390/rs12203457

Woods KD. 2000. Dynamics in late-successional hemlock–hardwood forests over three decades. Ecology. 81:110–126. https://doi.org/10.2307/177138

Woods KD. 2004. Intermediate disturbance in a late-successional hemlock–northern hardwood forest. J Ecol. 92:464–476. https://doi.org/10.1111/j.0022-0477.2004.00881.x

Woods KD, Kern CC. 2022. Intermediate disturbances drive long-term fluctuation in old-growth forest biomass: an 84-yr temperate forest record. Ecosphere. 13. https://doi.org/10.1002/ecs2.3871

Wulder MA et al. 2012. Lidar sampling for large-area forest characterization: A review. Remote Sens Environ. 121:196–209. https://doi.org/10.1016/j.rse.2012.02.001

Zhou B et al. 2011. The great 2008 Chinese ice storm: its socio-economic-ecological impact and sustainability lessons learned. Bull Am Meteorol Soc. 92:47–60. https://doi.org/10.1175/2010BAMS2857.1